

See discussions, stats, and author profiles for this publication at: <https://www.researchgate.net/publication/268076312>

Design, synthesis, and biological evaluation of quinazoline derivatives as α -glucosidase inhibitors

ARTICLE in MEDICINAL CHEMISTRY RESEARCH · NOVEMBER 2014

Impact Factor: 1.4 · DOI: 10.1007/s00044-014-1293-5

READS

133

11 AUTHORS, INCLUDING:



Venkateshwarlu Gurram

GVK Bio

11 PUBLICATIONS 20 CITATIONS

[SEE PROFILE](#)



Chiranjeevi Thulluri

Jawaharlal Nehru Technological University...

19 PUBLICATIONS 51 CITATIONS

[SEE PROFILE](#)



Pavan Kumar Machiraju

GVK Bio

13 PUBLICATIONS 40 CITATIONS

[SEE PROFILE](#)



Balaram Patro

GRK Research Laboratories, Hyderabad, India

53 PUBLICATIONS 408 CITATIONS

[SEE PROFILE](#)

Development of α -glucosidase inhibitors by room temperature C–C cross couplings of quinazolinones^t

Cite this: *Org. Biomol. Chem.*, 2013, **11**, 4778

Ramesh Garlapati,^{a,b} Narendra Pottabathini,^{*a} Venkateshwarlu Gurram,^a Kumara Swamy Kasani,^a Rambabu Gundla,^c Chiranjeevi Thulluri,^d Pavan Kumar Machiraju,^c Avinash B. Chaudhary,^a Uma Addepally,^d Raveendra Dayam,^c Venkata Rao Chunduri^b and Balaram Patro^a

Novel quinazolinone based α -glucosidase inhibitors have been developed. For this purpose a virtual screening model has been generated and validated utilizing acarbose as a α -glucosidase inhibitor. Homology modeling, docking, and virtual screening were successfully employed to discover a set of structurally diverse compounds active against α -glucosidase. A search of a 3D database containing 22 500 small molecules using the structure based virtual model yielded ten possible candidates. All ten candidates were *N*-3-pyridyl-2-cyclopropyl quinazolinone-4-one derivatives, varying at the 6 position. This position was modified by Suzuki–Miyaura cross coupling with aryl, heteroaryl, and alkyl boronic acids. A catalyst screen was performed, and using the best optimal conditions, a series of twenty five compounds was synthesized. Notably, the C–C cross coupling reactions of the 6-bromo-2-cyclopropyl-3-(pyridyl-3-ylmethyl)quinazolin-4(3*H*)-one precursor have been accomplished at room temperature. A comparison of the relative reactivities of 6-bromo and 6-chloro-2,3-disubstituted quinazolinones with phenyl boronic acid was conducted. An investigation of pre-catalyst loading for the reaction of the 6-bromo-2-cyclopropyl-3-(pyridyl-3-ylmethyl)quinazolin-4(3*H*)-one substrate was also carried out. Finally, we submitted our compounds to biological assays against α -glucosidase inhibitors. Of these, three hits (compounds **4a**, **4t** and **4r**) were potentially active as α -glucosidase inhibitors and showed activity with IC_{50} values $<20\ \mu M$. Based on structural novelty and desirable drug-like properties, **4a** was selected for structure–activity relationship study, and thirteen analogs were synthesized. Nine out of thirteen analogs acted as α -glucosidase inhibitors with IC_{50} values $<10\ \mu M$. These lead compounds have desirable physicochemical properties and are excellent candidates for further optimization.

Received 30th March 2013,
Accepted 20th May 2013

DOI: 10.1039/c3ob40636a

www.rsc.org/obc

Introduction

Diabetes mellitus is one of the most common and serious metabolic disorders, characterized by high blood-glucose levels which result from defects in insulin secretion, or action, or both.¹

Insulin enables cells to absorb glucose in order to turn it into energy. However, in diabetes, the body either does not respond properly to its own insulin or does not make enough

insulin, or both. This causes glucose to accumulate in the blood, which often leads to various complications, such as blindness, kidney failure, or microvascular disease, which could lead to atherosclerosis, strokes, and other coronary heart disease.² α -Glucosidase is an enzyme that catalyzes the exohydrolysis of 1,4- α -glucosidic linkages with release of α -glucose. α -Glucosidase inhibitors decrease the absorption of carbohydrates from the digestive tract, thereby lowering the after-meal glucose levels.³ For this reason, the α -glucosidase inhibitors are clinically used as oral antihyperglycemic agents to delay intestinal carbohydrate absorption and lessen postprandial increases in glucose levels.⁴ Some α -glucosidase inhibitors, such as acarbose, miglitol, and voglibose, are currently used in combination with either diet or other anti-diabetic agents to control the blood glucose levels of patients (Fig. 1). However, they often cause side effects such as flatulence and diarrhea. Hence, natural and synthesized α -glucosidase inhibitors have become an attractive therapeutic approach for the treatment of postprandial hyperglycemia.⁵ α -Glucosidase

^aMedicinal Chemistry Division, GVK Biosciences Pvt. Ltd, Plot 28A, IDA Nacharam, Hyderabad, India. E-mail: narendra.pottabathini@gvkbio.com;
Fax: +91 40 6628 1505; Tel: +91 40 6628 1275

^bDepartment of Chemistry, Sri Venkateswara University, Tirupathi, India

^cInformatics Division, GVK Biosciences Pvt. Ltd, Plot 79, IDA Mallapur, Hyderabad, India

^dCentre for Innovative Research, CBT, IST, JNTUH, Hyderabad, India

^tElectronic supplementary information (ESI) available: Copies of the ¹H NMR and ¹³C NMR spectra are for all key intermediates and final products; additional information as needed. See DOI: 10.1039/c3ob40636a

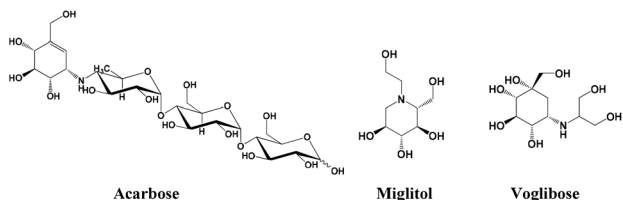


Fig. 1 Known iminosugars as inhibitors of α -glucosidase.

inhibitors are also known for anti-HIV, anticancer and other activities other than anti-diabetes.⁶

In this context we designed quinazolinone-based non-carbohydrate mimetic inhibitors of the α -glucosidase enzyme. C-6 substituted quinazolinone derivatives were screened as α -glucosidase inhibitors by *in silico* high-throughput screening. As the three dimensional structure of α -glucosidase is not available, it was derived through homology modeling. A virtual library of C-6 substituted quinazolinone derivatives was formed and docking simulation studies of C-6 substituted quinazolinone derivatives were performed using the MODELER program interfaced with Discovery Studio 3.5 (DS3.5). Among the designed compounds, three were found to be more potent than the standard drug acarbose.

Among the multitudinous biologically active heterocycles, nitrogen containing heterocycles play a vital role.⁷ In fact, recent surveys have reported that a large number of molecules currently under investigation by researchers contain nitrogen heterocycles, and of these, quinazoline and quinazolinone derivatives constitute the most important family of compounds.⁸ These quinazolines and quinazolinones have a common unique structural framework, which we were able to use as a scaffold for diversification, which in turn is useful for the preparation of pharmacological drugs.⁹ So far, research on quinazolin-4(3*H*)-ones has been carried out on the C-2, N-3 and C-4 positions of the core structure. A very few literature evidences have been studied on the extension of C-6 position of the core structure.¹⁰ Therefore, there has been a substantial amount of interest in developing efficient methods for the synthesis of C-6 substituted quinazolin-4(3*H*)-ones. Recently we communicated a facile palladium catalyzed synthetic method for the introduction of substituted amino groups at the C-6 position of 2-cyclopropyl-3-(pyridyl-3-ylmethyl)quinazolin-4(3*H*)-one with excellent yields.¹¹ In continuation of this work, we conducted an extensive study on C-C cross coupling reactions of 6-halo-2,3-disubstituted 3*H*-quinazolin-4-ones.

There are a few reports describing the C-C coupling of 6-halo substituted quinazolinones with moderate yields. Most of these approaches are limited and there are no reports of thorough study of Suzuki–Miyaura cross coupling reactions on this scaffold.¹² Herein we report an extensive study of Pd-catalyzed Suzuki–Miyaura cross coupling reactions at C-6 of 2-cyclopropyl-3-(pyridyl-3-ylmethyl)quinazolin-4(3*H*)-one in excellent yields. We explored the influence of catalytic systems on the efficiency of the cross coupling reactions and evaluated a much wider substrate scope than before. We also describe

C-C bond-forming reactions at the C-6 position of 2,3-disubstituted quinazolin-4(3*H*)-ones using both C-6 bromo and chloro quinazolin-4(3*H*)-one derivatives under mild, room temperature conditions to install C-6 aryl/alkyl/heteroaryl groups. To our knowledge, room temperature reactions at the C-6 position of quinazolin-4(3*H*)-ones have not been reported to date. In the broader context, accomplishing such reactions under ambient temperatures generally represents a nontrivial undertaking. In addition, we also compared the reactivities of C-6 bromo and chloro quinazolin-4(3*H*) ones, and evaluated the pre-catalyst loading effect on reaction productivity. Furthermore, this report also demonstrates the stability of the cyclopropyl moiety to the Suzuki–Miyaura cross coupling reaction conditions.¹³

Finally, we submitted our compounds to biological assays against α -glucosidase inhibitors.

Results and discussion

Molecular modeling

Structure based virtual screening. Structure based virtual screening was performed against the homology modeled α -glucosidase protein using an in-house database (22 500 compounds). The in-house database is filtered using a multiple property filter, Lipinski's rule, and ADMET, to prioritize compounds with higher probabilities of possessing favourable tissue absorption distribution profiles. The last step of screening involves a Pose filter using Schrödinger docking post-processing, it is possible to simply filter the output file of docked poses according to whether or not they fulfil certain receptor ligand contacts or interactions. Each compound, docked into the active site, was visually inspected, and those displaying unfavourable interactions within the binding site were discarded. Finally, ten compounds with high docking scores and reasonable hydrogen bond interactions were synthesized by either room temperature or elevated temperature C-C cross-coupling reactions. These compounds were submitted for biological testing; from these ten compounds, three compounds showed reasonable biological activity against α -glucosidase. A flow diagram for structure based virtual screening is shown in Fig. 2.

From the sequence alignment of templates and target protein, the key active site residues Asp199, Asp321, Arg517 and His591 are conserved in α -glucosidase and maltase-glucoamylase (Asp203, Asp327, Arg526 and His600 from 2QLY, 3L4T). The Ramachandran plot for the predicted model reveals that 90% residues were found in most favourable region, while 8.2% were found in the allowed region (see the Experimental section for figure). The other violations for bond lengths, amide torsions, side chain torsions and backbone torsions showed any major deviations from the allowed values. Only 0.8% of residues were in the disallowed region, yet these residues were not located in the active site. The overall G factor calculated on basis of the main chain parameter implied that the modeled structure was acceptable for virtual screening.

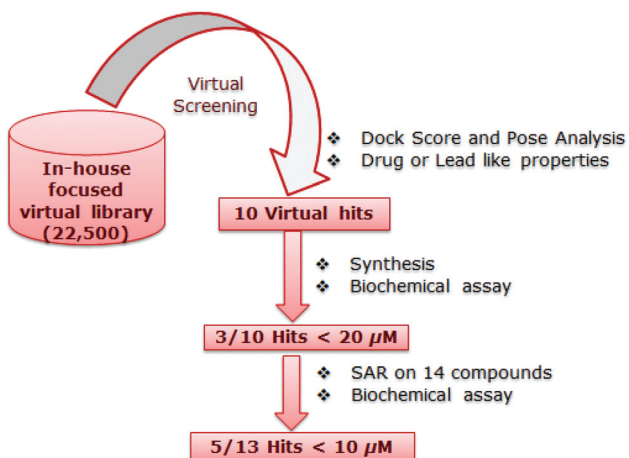


Fig. 2 Schematic representation of *in silico* screening protocol implemented in the discovery of α -glucosidase inhibitors.

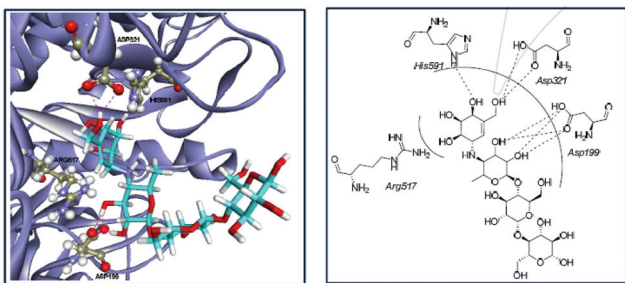


Fig. 3 (a) Predicted binding mode of acarbose in modeled protein (3D representation). (b) Predicted binding mode of acarbose.

The predicted binding mode of acarbose against the α -glucosidase model also retained hydrogen bond interactions with conserved amino acids *i.e.* three hydrogen bond interactions with the Asp321, His591, and Asp199 residues of the homology modeled protein. The first hydrogen bond is observed between the hydroxyl group of acarbose and the COO group of the Asp321 residue ($-\text{OH}\cdots\text{O}-\text{CO}$, 2.44 Å). The second hydrogen bond is observed between the hydroxyl group of the compound and the N-H of His591 ($-\text{HO}\cdots\text{HN}$, 1.73 Å). The third hydrogen bond is observed between the hydroxyl group of the compound and the COO group of the Asp199 residue ($-\text{OH}\cdots\text{O}-\text{CO}$, 1.77 Å). The predicted binding mode and 2D interaction diagram of acarbose in the homology modeled α -glucosidase protein are shown in Fig. 3a and 3b.

Structure based virtual screening yielded ten compounds from in-house virtual library compounds. These ten compounds were synthesized and submitted for biological testing (Fig. 4). Out of ten compounds, three compounds showed $< 20 \mu\text{M}$ inhibitory activity against α -glucosidase and the remaining are not active (NA) against α -glucosidase.

The analog **4r** showed $\sim 5.75 \mu\text{M}$ inhibitory activity against α -glucosidase and the predicted binding mode has a hydrogen bond between nitrogen in the indole group of compound **4r**

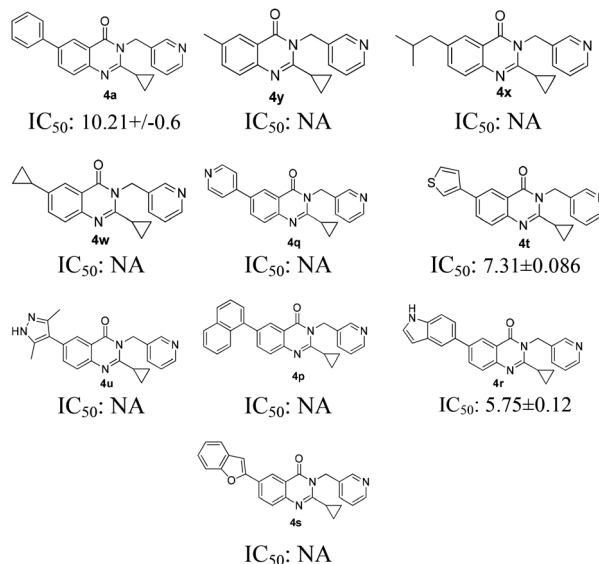


Fig. 4 First set of ten compounds after virtual screening with α -glucosidase inhibitory activity, including biological assay results; IC₅₀ values are in μM .

and the side chain OH group of the Ser593 residue ($-\text{OH}\cdots\text{N}$, 2.16 Å). Compound **4t** showed $\sim 7.31 \mu\text{M}$ inhibitory activity against α -glucosidase and the predicted binding mode has a hydrogen bond between nitrogen in the pyridine moiety of **4t** and the guanidine hydrogen of the Arg517 residue ($-\text{N}\cdots\text{H}-\text{N}$, 2.00 Å). Compound **4a** showed $\sim 10.21 \mu\text{M}$ inhibitory activity against α -glucosidase and the predicted binding mode has a hydrogen bond between the carbonyl group of **4a** and the guanidine hydrogen of the Arg517 residue ($-\text{CO}\cdots\text{H}-\text{N}$, 2.89 Å). The predicted binding mode of these three compounds with the homology modeled protein is shown in Fig. 5.

From the biological testing, 2-cyclopropyl-6-phenyl-3-((pyridin-3-yl)methyl)quinazolin-4(3*H*)-one (**4a**) was considered further to explore the relevance of various structural elements. We designed fourteen analogs of **4a** by substituting different groups on the phenyl moiety present at the C-6 position of quinazolin-4(3*H*)-one (Table 1).

3,4-Dimethylphenyl substituted analog **4c** ($7.44 \mu\text{M}$), 3-fluoro-4-methylphenyl **4e** ($5.75 \mu\text{M}$) and 3,4-dihydroxyphenyl substituted quinazolinone **4n** ($7.68 \mu\text{M}$) showed slight increases in inhibitory activity against α -glucosidase. 2,4-Dihydroxyphenyl substituted derivative **4m** ($6.527 \mu\text{M}$) showed higher activity compared to 3,4-dihydroxy substituted phenyl derivative **4n**. The trihydroxyphenyl substituted derivative, **4o** ($5.70 \mu\text{M}$) showed the second highest inhibitory activity against α -glucosidase among all the synthesized compounds. The 2,6-dichloro substituted quinazolinone derivative **4f** showed the highest inhibition against α -glucosidase. The derivatives of compound **4a** along with their docking scores and biological activities are given in Table 1. From the predicted binding mode of compound **4o**, it is clear that it forms two hydrogen bond interactions with the protein. The first hydrogen bond is observed between the hydroxyl group at the fourth position of the phenyl moiety present in the compound

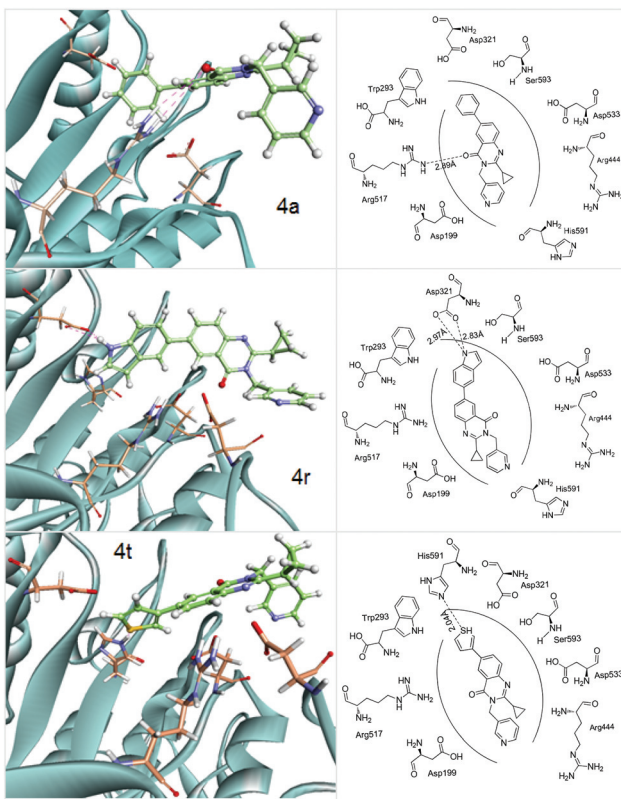


Fig. 5 Predicted binding mode of **4a**, **4r**, and **4t** in modeled protein in a 3D representation along with 2D representations.

Table 1 IC₅₀ values (μM), dock scores for 6-phenylquinazolin-4(3*H*)-one derivatives against α -glucosidase

Entry	Compound code	R	Docking score	IC ₅₀ (μM) of α -glucosidase
1	4a	H	-8.15	10.21 ± 0.6
2	4b	2-OCH ₃	-6.23	NA
3	4c	3,4-Dimethyl	-9.57	7.44 ± 0.73
4	4d	2-COCH ₃	-8.15	NA
5	4e	3-F and 4-CH ₃	-9.13	7.57 ± 0.41
6	4f	2,6-Dichloro	-9.79	4.04 ± 0.049
7	4g	4-CO ₂ CH ₃	-7.87	NA
8	4h	4-CN	-8.26	NA
9	4i	3-NO ₂	-7.68	NA
10	4j	4-NMe ₂	-8.93	NA
11	4l	4-SO ₂ Me	-7.93	NA
12	4m	2,4-Di-OH	-9.89	6.52 ± 0.41
13	4n	3,4-Di-OH	-8.86	7.68 ± 0.06
14	4o	2,3,4-Tri-OH	-9.18	5.70 ± 0.09
15	Acarbose	Standard		6.04 ± 0.17

All the test compounds were dissolved in DMSO to required concentration; the test concentrations used were 2–10 μM .

4o and the electron rich oxygen in the COO group of the Asp321 residue ($-\text{OH}\cdots\text{O}-\text{CO}$, 2.20 Å). The second hydrogen bond is observed between the hydroxyl group at the third

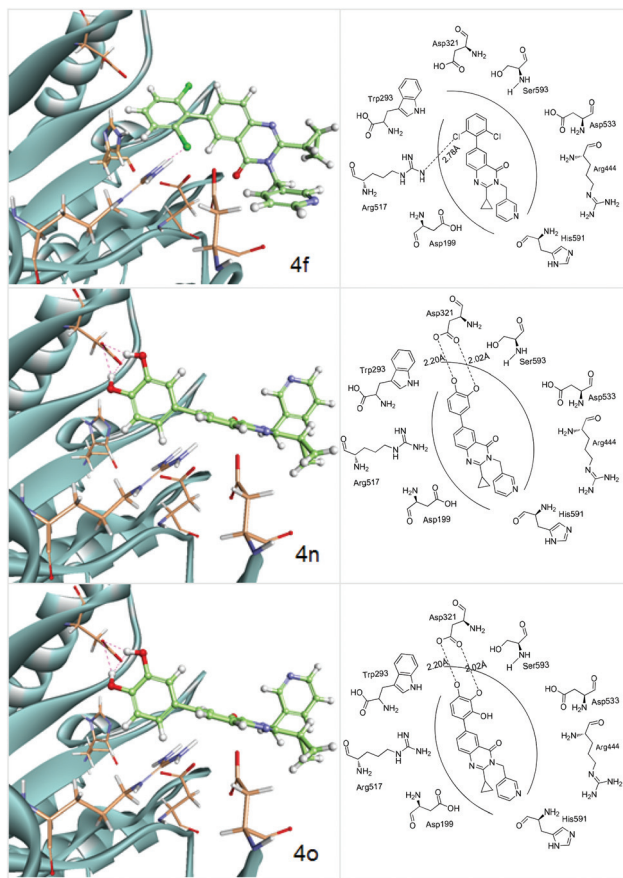


Fig. 6 Predicted binding mode of **4f**, **4n**, and **4o** in modeled protein 3D representation along with 2D representation.

position of the phenyl moiety present in compound **4o** and the carbonyl group in the COO group of Asp321 ($-\text{OH}\cdots\text{OC}-\text{O}$, 2.02 Å). The predicted binding mode of compound **4o** with the homology modeled protein is shown in Fig. 6.

Chemistry

The development of easily applicable synthetic strategies for the construction of carbon–carbon bonds with palladium catalyzed Suzuki–Miyaura cross-coupling reactions remains an important challenge in organic synthesis.¹⁴ 6-Bromo- and 6-chloro-2-cyclopropyl-3-(pyridyl-3-ylmethyl)quinazolin-4(3*H*)-ones were chosen for the present study. The overall aim was not only to determine the best conditions for Suzuki–Miyaura cross coupling reactions of both precursors, but also to find the optimal conditions that can be applied for the synthesis of a broad range of 6-aryl, heteroaryl, and alkyl 2,3-disubstituted quinazolinones. Both halo quinazoline-4(3*H*)-one precursors **3a** and **3b** (Fig. 7) are conveniently synthesized in two steps by known procedures (see the ESI† for details).

We have previously utilized precursors **3a**, **3b** for amination reactions. We followed similar screening reactions as described in our recent communication on C–C cross-coupling reactions of O⁶-alkyl-2-haloinosine derivatives.¹⁵ Optimization experiments were carried out using Pd(OAc)₂ and Pd₂(dba)₃ as

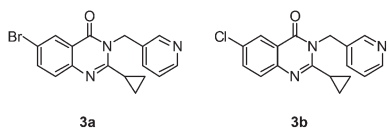


Fig. 7 6-Halo-2-cyclopropyl-3-(pyridyl-3-ylmethyl)quinazolin-4(3*H*)-ones selected for analysis.

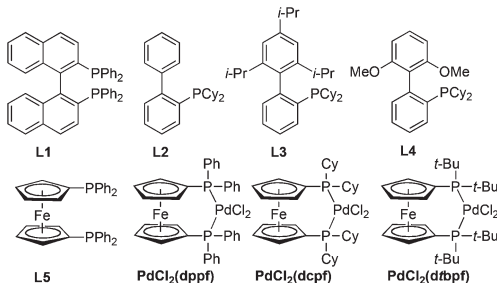


Fig. 8 Five ligands and three Pd(II) pre-catalysts selected for the initial analysis.

metal sources, ligands **L1–L5** were selected for combination with the metal, and three ferrocenyl Pd(II) pre-catalysts (Fig. 8) were selected for analysis.

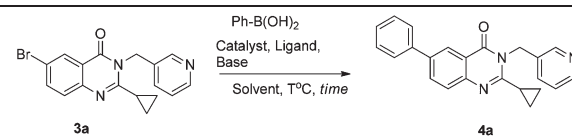
The optimization experiments were performed with phenyl boronic acid at room temperature for 36 h. We screened conditions with K_3PO_4 as base and also compared with several solvents (PhMe, 1,4-dioxane and THP). Precursor **3a** was only partially soluble in toluene; THP was superior to 1,4-dioxane.¹⁶ Results from our initial investigations are shown in Tables 2 and 3. From these data, $Pd(OAc)_2/\mathbf{L}2$ (CyJohnPhos) was superior to the other biaryl-ligand-based catalysts, which gave product yields in the range of 40–68% with a catalytic loading of metal of 5 or 10 mol%.

Among the ferrocene-based pre-catalysts that were tested, $[PdCl_2(dcpf)]$ and $[PdCl_2(d^tbpf)]$ were found to be the best, and were superior to $Pd(OAc)_2/\mathbf{L}2$.

THP was a generally better solvent as compared to 1,4-dioxane. The reaction of 5 mol% $[PdCl_2(dcpf)]$ in the presence of THP was superior compared to 1,4-dioxane at room temperature. Whereas, in the case of 5 mol% $[PdCl_2(d^tbpf)]$, THP and 1,4-dioxane were both good solvents. Room temperature reactions were carried out with 10 or 20 mol% of catalyst using THP as solvent and the results are tabulated in Table 3. Finally, $[PdCl_2(d^tbpf)]$ was determined to be a slightly better catalytic system compared to $[PdCl_2(dcpf)]$. The cost of $[PdCl_2(d^tbpf)]$ is higher than $[PdCl_2(dcpf)]$, so we have considered $[PdCl_2(dcpf)]$ for the evaluation of C–C cross coupling with different boronic acids. The C–C cross coupling reactions yields didn't change appreciably when the reactions were conducted over 36 h.

After finalizing the optimal conditions, several boronic acids underwent cross coupling reactions at room temperature to synthesize the analogs shown in Table 1. From Table 1, it is clear that a wide assortment of aryl, heteroaryl and alkyl boronic acids undergo Pd-catalyzed Suzuki–Miyaura cross coupling reactions.

Table 2 Initial optimization of C–C reaction experiments on **3a** at room temperature^{a,b}

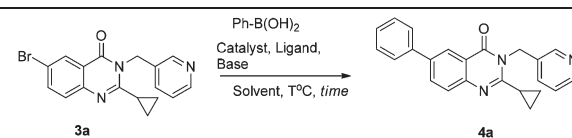


Entry	Catalytic system, conditions, $T = rt$, $t = 36\text{ h}$	Yield ^c (%)
1	5 mol% $[PdCl_2(dcpf)]/K_3PO_4$, 1,4-dioxane	20
2	5 mol% $[PdCl_2(dcpf)]/K_3PO_4$, THP	84
3	5 mol% $[PdCl_2(d^tbpf)]/K_3PO_4$, 1,4-dioxane	79
4	5 mol% $[PdCl_2(d^tbpf)]/K_3PO_4$, THP	83
5	5 mol% $[PdCl_2(dppf)]/K_3PO_4$, THP	15
6	5 mol% $Pd(OAc)_2/7.5\text{ mol\% } \mathbf{L}1/K_3PO_4$, THP	19
7	5 mol% $Pd(OAc)_2/7.5\text{ mol\% } \mathbf{L}2/K_3PO_4$, THP	55
8	5 mol% $Pd(OAc)_2/7.5\text{ mol\% } \mathbf{L}3/K_3PO_4$, THP	41
9	5 mol% $Pd_2(dbu)_3/7.5\text{ mol\% } \mathbf{L}4/K_3PO_4$, THP	50
10	5 mol% $Pd(OAc)_2/7.5\text{ mol\% } \mathbf{L}5/K_3PO_4$, THP	21

^a Reaction conditions (entries 1–10) **3a** precursor 0.0711 mM in anhydrous solvent, 2.0 molar equiv. Ph-B(OH)₂, 2.0 molar equiv. of base. ^b Reactions were conducted in closed vial sparged with argon.

^c % yields refer to isolated and purified products.

Table 3 Initial optimization of C–C reaction experiments on **3a** at room temperature^{a,b}



Entry	Catalytic system, conditions, $T = rt$, $t = 36\text{ h}$	Yield ^c (%)
1	10 mol% $[PdCl_2(dcpf)]/K_3PO_4$, THP	89
2	10 mol% $[PdCl_2(d^tbpf)]/K_3PO_4$, THP	95
3	20 mol% $[PdCl_2(dcpf)]/K_3PO_4$, THP	92
4	20 mol% $[PdCl_2(d^tbpf)]/K_3PO_4$, THP	95
5	10 mol% $[PdCl_2(dppf)]/K_3PO_4$, THP	28
6	10 mol% $Pd(OAc)_2/15\text{ mol\% } \mathbf{L}1/K_3PO_4$, THP	28
7	10 mol% $Pd(OAc)_2/15\text{ mol\% } \mathbf{L}2/K_3PO_4$, THP	68
8	10 mol% $Pd(OAc)_2/15\text{ mol\% } \mathbf{L}3/K_3PO_4$, THP	55
9	10 mol% $Pd_2(dbu)_3/15\text{ mol\% } \mathbf{L}4/K_3PO_4$, THP	58
10	10 mol% $Pd(OAc)_2/15\text{ mol\% } \mathbf{L}5/K_3PO_4$, THP	24

^a Reaction conditions (entries 1–10) **3a** precursor 0.0711 mM in anhydrous solvent, 2.0 molar equiv. Ph-B(OH)₂, 2.0 molar equiv. of base. ^b Reactions were conducted in closed vial sparged with argon.

^c % yields refer to isolated and purified products.

The final C–C coupling products of boronic acids with electron donating groups like 3,4-dimethyl phenyl boronic acid (entry 3, 81%), *o*-methoxy phenylboronic acid (entry 2, 88%) and sterically hindered 2,6-dichlorophenyl boronic acid (entry 6, 89%) were produced in excellent yields. The naphthalene system also resulted in a good yield (entry 16, 79%). Even when strongly electron depleting substituents were present (*m*-nitro, *o*-acetyl), good yields were obtained. Reactions of boronic acids with electron withdrawing groups like 4-cyano-phenyl boronic acid (entry 8, 59%), fluorinated substituents like 3-fluoro-4-methyl (entry 5, 90%) and bis(3,5-trifluoromethyl) phenyl boronic acids (entry 11, 66%) also resulted in

Table 4 Evaluation of the scope of C–C coupling reactions of various boronic acids with 6-bromo- and 6-chloro-3-(pyridyl-3-ylmethyl)quinazolin-4(3*H*)-ones, **3a** and **3b**^a

Entry	Amine	Product	rt, 36 h,	80 °C, 8 h, 1,4-dioxane, yield ^c (%)
			THP, yield ^b (%)	
1		4a	92	97 (82) ^d
2		4b	88	98 ^d
3		4c	81	85 (56) ^d
4		4d	80	92
5		4e	90	97 (61) ^d
6		4f	89	98
7		4g	56	89 (56) ^d
8		4h	59	98 (67) ^d
9		4i	62	97
10		4j	60	75
11		4k	66	71
12		4l	NR	58
13		4m	NR	88 ^e
14		4n	NR	86 ^e
15		4o	NR	75 ^e
16		4p	79	85
17		4q	NP	81 (35) ^d

Table 4 (Contd.)

X= Br; 3a				
X= Cl; 3b				
		4a - 4y		
Entry	Amine	Product	rt, 36 h, THP, yield ^b (%)	80 °C, 8 h, 1,4-dioxane, yield ^c (%)
18		4r	NP	90 (86) ^d
19		4s	82	88
20		4t	60	85 (69) ^d
21		4u	NR	96
22		4v	NP	55
23		4w	NP	65 (82) ^d
24		4x	NP	87
25		4y	25	91 (83) ^d

^a Reaction conditions (entries 1–25) bromo and chloro compound (**3a**, **3b**) 0.0711 mM in anhydrous. ^b 2 molar equiv. boronic acid, 2.0 equiv. K₃PO₄, 20 mol% of PdCl₂(dcpf), reactions were conducted in closed vial sparged with argon at rt. ^c 1.5 molar equiv. boronic acid, 2.0 equiv. K₃PO₄, 20 mol% of PdCl₂(dcpf), 80 °C, reactions were conducted in closed vial sparged with argon. % yields refer to isolated and purified products. ^d Yield obtained with chloro substrate **3b**. ^e Final compound synthesized in two steps, C–C coupling followed by deprotection of methyl group. NR: no reaction; NP: not performed.

good yields. Reactions with heteroaryl boronic acids resulted in moderate to good yields from 60% to 82% (entries 17 to 22). In a few cases unreacted Br-precursor **3a** remained in the reaction. The reaction with methyl boronic acid resulted a low yield (entry 25, 25%). Thus, we decided to examine the cross coupling reactions of aliphatic boronic acids and heteroaryl boronic acids at elevated temperatures for the completion of reaction, to generate material for biological assays.

At this stage, we again explored the generality of the elevated temperature cross coupling reaction conditions, and [PdCl₂(dcpf)] proved the best catalytic system.

Comparison of the product formation dependent on the pre-catalyst loading

We investigated the effect of pre-catalyst loading on the reaction of 6-bromo precursor (**3a**) with phenyl boronic acid, drawing an interesting observation. Fig. 9 shows the reaction rate comparison for the formation of **4a**. The rate of reaction is dependent on the catalyst loading. The reactions were

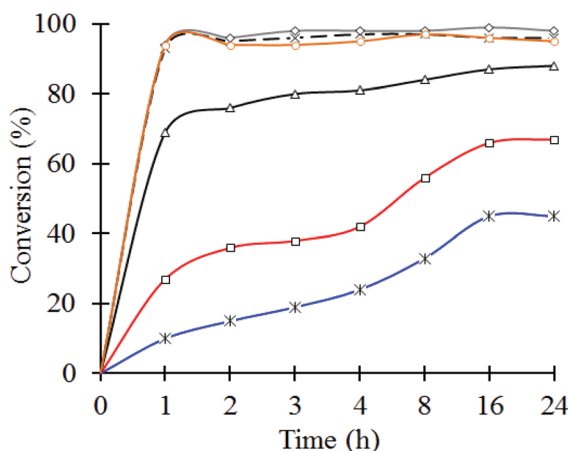


Fig. 9 Comparison of the formation of **4a** with (—x—) 1 mol%, (—□—) 2 mol%, (—△—) 5 mol%, (—×—) 10 mol%, (—○—) 20 mol%, (——) 30 mol%; mol% of pre-catalyst loading on **3a** with $\text{PhB}(\text{OH})_2$ at 80 °C. Formation of **4a** in percentages, determined by LC/MS. K_3PO_4 as base and 1,4-dioxane as solvent.

conducted with 2.0 molar eq. K_3PO_4 in 1,4-dioxane at 80 °C. All the six reactions were performed with different pre-catalyst loadings of 1 mol%, 2 mol%, 5 mol%, 10 mol%, 20 mol% and 30 mol% in a parallel reactor. LC/MS analyses of all reactions were taken at different time intervals *i.e.* 1 h, 2 h, 3 h, 4 h, 8 h, 16 h and 24 h. Reactions yields were improved significantly from 1 mol% to 10 mol%. It was also observed that increasing the catalytic loading from 10 mol% to 30 mol% didn't result a change in yield in the case of $\text{PhB}(\text{OH})_2$.

Relative reactivities of bromo quinazolinone (**3a**) and chloro quinazolinone (**3b**)

It is evident that **3a** is superior to **3b** in terms of product yield under the C–C bond forming reaction conditions (Table 4). We decided to determine their relative reactivities in a competitive experiment.

We conducted a reaction of an equimolar amount of **3a** and **3b** (1.5 molar equiv. each) with one molar equivalent of phenyl boronic acid, under the optimized conditions. After the complete consumption of phenyl boronic acid the experiment was stopped. Product **4a** as well as reactants **3a**, **3b** were collected together by column chromatography and subjected to LC/MS analysis.

In the mixture, 12.3% of the bromo quinazolinone **3a** and 47% of the chloro quinazolinone **3b** was observed. **3b** was totally non-reactive and the total quantity was recovered after the reaction. This experiment shows two important factors. First, that C-6 bromo quinazolinone precursor **3a** is more rapidly consumed than chloro analog **3b**, and second, reductive dehalogenation does not appear to be significant. Fig. 10 shows the LC trace of the reaction mixture from the competition experiment. The LC/MS analysis data can be found in the ESI.† Suzuki reactions with Cl precursor (**3b**) have a higher activation energy due to the greater Ar–Cl bond strength compared to Ar–Br, so lower reactivity is expected.

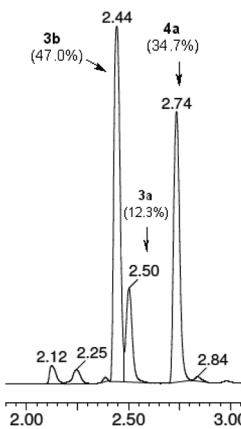


Fig. 10 LC analysis of the reaction mixture from a competitive reaction of **3a** and **3b** with $\text{PhB}(\text{OH})_2$ (showing the integrated percentages).

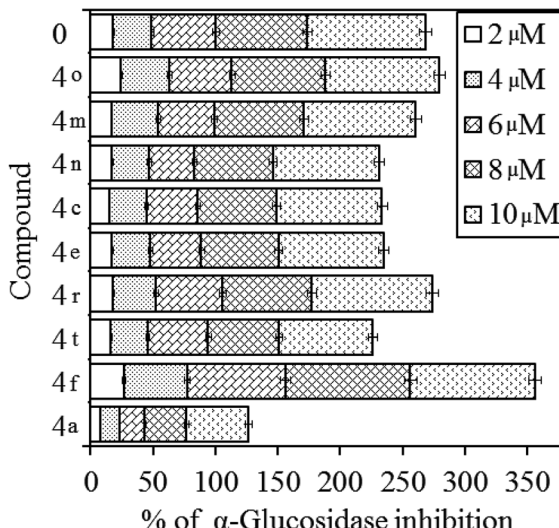


Fig. 11 The effect of inhibitor dosage on the response of α -glucosidase inhibition. The concentrations of test compounds employed from lower to higher (2 μM to 10 μM) to study the inhibition of α -glucosidase.

In vitro functional activity of selected analogs

All the synthesized compounds were evaluated for their *in vitro* α -glucosidase inhibition activity, and the inhibitory effects of the positive test compounds were concentration dependent. Typical dose-response plots of α -glucosidase inhibition for the constructed molecules are shown in Fig. 11. The response of enzyme inhibition increased with increasing dosage of the active compounds. Among 25 *in vitro* screened molecules, 9 molecules showed IC_{50} concentrations below 10 μM . In the graph (Fig. 11), each fragment of the column corresponds to a specific concentration of the respective compound. The α -glucosidase inhibitor assay was analyzed by Dixon plot at two different substrate concentrations (1 mM and 2 mM) corresponding to two different $-K_i$ values (-2.32 and -1.96) for the active inhibitors, **4f** and **4o** (Fig. 12 and 13).

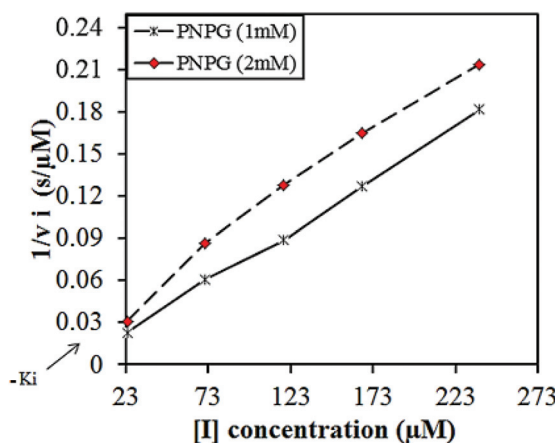


Fig. 12 Dixon plot of reciprocal rates of metabolite ($1/v$) formation as a function of inhibitor [I] (compound **4f**) concentrations.

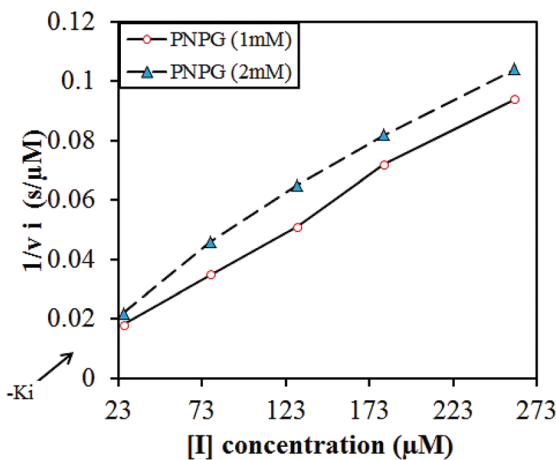


Fig. 13 Dixon plot of reciprocal rates of metabolite ($1/v$) formation as a function of inhibitor [I] (compound **4o**) concentrations.

Enzyme inhibition data were expressed as IC_{50} values (the concentration of the inhibitor required to produce 50% inhibition of the test models). From the results, the apparent IC_{50} values of the test compounds with respect to α -glucosidase activity were estimated. In the course of the screening study on α -glucosidase inhibitors, we found that the analogs synthesized showed different inhibitory activities against the enzyme.

Among 25 screened 2,3-disubstituted quinazolino-4(*3H*)-one molecules, 9 molecules showed fruitful inhibition. In comparison with acarbose, the test compounds **4f**, **4o**, and **4r** showed promising α -glucosidase inhibitory effect. Acarbose was used as reference compound.¹⁷

Conclusions

Pd-catalyzed C–C bond formation is effective for the introduction of substituted aryl/alkyl/heteroaryl groups at the C-6 position of 2-cyclopropyl-3-(pyridyl-3-ylmethyl)quinazolin-4(*3H*)-ones both at room temperature and elevated temperature. The combination of 10 mol% (dcpf)PdCl₂/K₃PO₄ in 1,4-dioxane gave good to excellent yields in the coupling of 6-bromo and 6-chloro-2-cyclopropyl-3-(pyridyl-3-ylmethyl)quinazolin-4(*3H*)-one with a variety of aryl, heteroaryl and alkyl boronic acids. The methodology for the C–C cross coupling appears to be broad in scope for 2,3-disubstituted quinazoline-4-ones. To our knowledge, this is the first report on successful C–C bond forming reactions at the C-6 position of 2,3-disubstituted quinazoline-4(*3H*)-ones at room temperature. In particular, a cyclopropyl substituent was shown to be stable under the Suzuki–Miyaura cross coupling conditions. Finally, we have studied the relative reactivities of the bromo and chloro quinazolinone precursors towards C–C cross coupling and it was clear that former is superior. We have also been investigated the pre-catalyst loading towards the reactivity of C–C cross coupling reactions and 10 mol% is suitable for phenyl boronic acid. The combination of these docking experiments and the development of facile chemical synthesis gives access to the development of other analogs as α -glucosidase inhibitors for further research which is being pursued in our laboratory.

position of 2-cyclopropyl-3-(pyridyl-3-ylmethyl)quinazolin-4(*3H*)-ones both at room temperature and elevated temperature. The combination of 10 mol% (dcpf)PdCl₂/K₃PO₄ in 1,4-dioxane gave good to excellent yields in the coupling of 6-bromo and 6-chloro-2-cyclopropyl-3-(pyridyl-3-ylmethyl)quinazolin-4(*3H*)-one with a variety of aryl, heteroaryl and alkyl boronic acids. The methodology for the C–C cross coupling appears to be broad in scope for 2,3-disubstituted quinazoline-4-ones. To our knowledge, this is the first report on successful C–C bond forming reactions at the C-6 position of 2,3-disubstituted quinazoline-4(*3H*)-ones at room temperature. In particular, a cyclopropyl substituent was shown to be stable under the Suzuki–Miyaura cross coupling conditions. Finally, we have studied the relative reactivities of the bromo and chloro quinazolinone precursors towards C–C cross coupling and it was clear that former is superior. We have also been investigated the pre-catalyst loading towards the reactivity of C–C cross coupling reactions and 10 mol% is suitable for phenyl boronic acid. The combination of these docking experiments and the development of facile chemical synthesis gives access to the development of other analogs as α -glucosidase inhibitors for further research which is being pursued in our laboratory.

Experimental section

Homology modeling and validation

Human lysosomal α -glucosidase amino acid sequence (FASTA format) was retrieved from the manually annotated and reviewed Swiss-Prot database (Swiss-Prot: P10253). The template search was performed using the BLAST-P program. The human maltase-glucoamylase (PDBID: 2QLY and 3L4T) two reference sequences were selected from the BLAST-P program (Fig. 14). α -Glucosidase has 44% sequence identity with two templates (PDBID: 2QLY and 3L4T) with query coverage of 90% for each. The three-dimensional (3D) model lysosomal α -glucosidase is constructed from 89 to 952 amino acid residues using human maltase-glucoamylase (PDBID: 2QLY and 3L4T) as template by the MODELER program interfaced with Discovery Studio 3.5 (DS3.5). MODELER implements comparative protein structure modeling by agreement with spatial restraints.¹⁸ The 3D model is obtained by the optimal

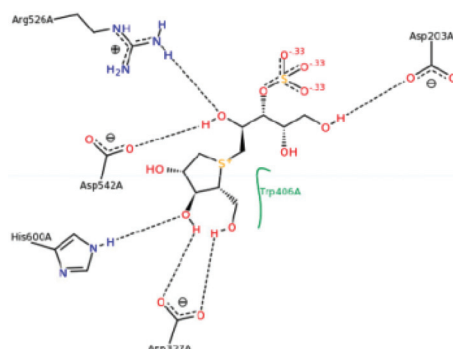


Fig. 14 Ligand Plot of 3L4T.

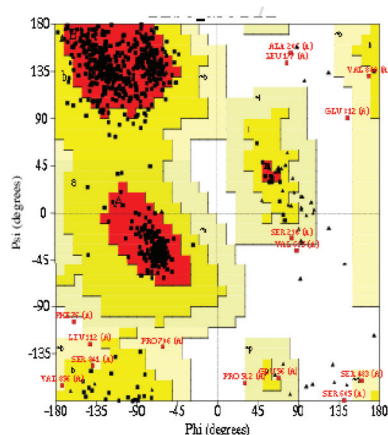


Fig. 15 Ramachandran plot of ψ/Φ ligand.

satisfaction of spatial restraints of homology-derived and stereochemically derived restraints from the alignment, and expressed in terms of probability density function of featured restraints. The stereochemical quality of the α -glucosidase homology model was validated by Ramachandran plot analysis performed using the PROCHECK program (Fig. 15).¹⁹

Docking studies

The docking studies were performed using Glide (Schrödinger) and the favourable interactions between one or more ligand molecules with receptor were analysed. In Glide, the combination of position and orientation of a ligand relative to the receptor, along with its conformation in flexible docking, is referred to as a ligand pose. The ligand poses that Glide generates pass through a series of hierarchical filters that evaluate the ligand's interaction with the receptor.

The initial filters test the spatial fit of the ligand to the defined active site, and examine the complementarity of ligand-receptor interactions using a grid-based method patterned after the empirical ChemScore function. Poses that pass these initial screens enter the final stage of the algorithm, which involves evaluation and minimization of a grid approximation to the OPLS-AA non bonded ligand-receptor interaction energy.²⁰ Final scoring is then carried out on the energy-minimized poses. By default, Schrödinger's proprietary GlideScore multi-ligand scoring function is used to score the poses. If GlideScore was selected as the scoring function, a composite Emodel score is then used to rank the poses of each ligand and to select the poses to be reported to the user (Fig. 16).

Docking simulations were performed using Glide program with OPLS-AA force field. The binding region was defined using a grid of $14 \text{ \AA} \times 14 \text{ \AA} \times 14 \text{ \AA}$ box centred on the centroid of the overlaid ligand on to the modeled 3D structure of protein, in order to confine the centroid of the docked inhibitor. Default settings were used for all the remaining parameters.

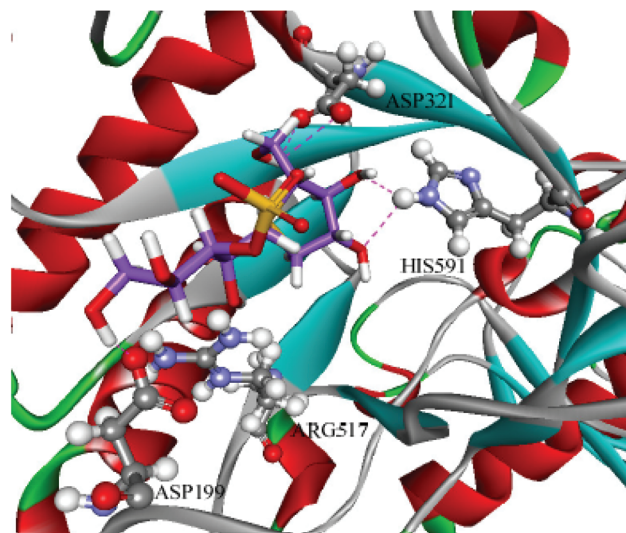


Fig. 16 Modeled human α -glucosidase.

General experimental considerations

Thin-layer chromatography was performed on 250 mm silica plates and column chromatographic purifications were performed on 100–200 mesh silica gel. All boronic acids, Pd(OAc)₂, Pd₂(dba)₃, ligands L1–L5, PdCl₂(dppf), PdCl₂(dpbf), and PdCl₂(d'bpbf), and all other reagents were obtained from commercial suppliers and were used without further purification. 1,4-Dioxane was distilled over NaBH₄ and then stored over Na. Prior to each reaction 1,4-dioxane was freshly distilled. For syntheses of compounds 3a, and 3b as well as their precursors, please see the ESI.† ¹H NMR spectra were collected either at 400 MHz or at 300 MHz and spectra are referenced to residual protio solvent. ¹³C NMR spectra, collected either at 100 MHz or at 75 MHz, are referenced to the carbon resonance of the deuterated solvent. Spectra were obtained either in de-acidified CDCl₃ (deacidification was performed by percolating the solvent through a bed of solid NaHCO₃ and basic alumina) or in DMSO-d₆ (see specific compound descriptions below). High resolution mass spectrometry was performed at the Mass Spectrometry Laboratory at GVK Biosciences Pvt Ltd. LC/MS analyses were performed with electrospray ionization (ESI), and operated in the positive ion mode. LC analysis was performed using a diode array detector.

General procedure for the cross coupling of the 6-bromo-2-cyclopropyl-3-(pyridin-3-ylmethyl)quinazolin-4(3*H*)-one at room temperature. In an oven dried, screw-cap vial equipped with a stirring bar were placed 6-bromo-2-cyclopropyl-3-(pyridin-3-ylmethyl)quinazolin-4(3*H*)-one (1 eq.), boronic acid (2.0 eq.), and K₃PO₄ (2 eq.), dissolved in anhydrous 1,4-dioxane (10 V). The vial was flushed with argon and, after addition of PdCl₂(dcpf) (0.2 eq.), sealed with a teflon-lined cap and placed in a sand bath that was maintained at room temperature. The reaction was monitored by TLC. Upon completion (36 h), the mixture was diluted with CH₂Cl₂. The mixture was washed with water and the organic layer was separated and

dried over Na_2SO_4 . Evaporation under reduced pressure provided the crude product, which was loaded onto a silica column packed in CH_2Cl_2 . Sequential elution with pet-ether, followed by 70% EtOAc in pet-ether, afforded the requisite compound. Finally, compounds were dried under high vacuum to remove traces of solvent (see specific compound headings below for details).

General procedure for the cross coupling of the 6-bromo and chloro-2-cyclopropyl-3-(pyridin-3-ylmethyl)quinazolin-4-(3H)-one. In an oven dried, screw-cap vial equipped with a stirring bar were placed 6-bromo or chloro -2-cyclopropyl-3-(pyridin-3-ylmethyl)quinazolin-4(3H)-one (1 eq.), boronic acid (1.5 eq.), and K_3PO_4 (2 eq.), dissolved in anhydrous 1,4-dioxane (10 V). The vial was flushed with argon and, after addition of $\text{PdCl}_2(\text{dpdf})$ (0.2 eq.), sealed with a teflon-lined cap and placed in a sand bath that was maintained at 80 °C. The reaction was monitored by TLC. Upon completion (8 h), the mixture was cooled and diluted with CH_2Cl_2 . The mixture was washed with water and the organic layer was separated and dried over Na_2SO_4 . Evaporation under reduced pressure provided the crude product, which was loaded onto a silica column packed in CH_2Cl_2 . Sequential elution with pet-ether, followed by 70% EtOAc in pet-ether, afforded the requisite compound. Finally, compounds were dried under high vacuum to remove traces of solvent (see specific compound headings below for details).

2-Cyclopropyl-6-phenyl-3-(pyridin-3-ylmethyl)quinazolin-4-(3H)-one (4a). Chromatography was performed using 70% EtOAc in *n*-hexane to yield a pale yellow solid. R_f (70% EtOAc in *n*-hexane) = 0.55; ^1H NMR (300 MHz, DMSO- d_6): δ = 8.61 (s, 1H), 8.51 (d, J = 3.3 Hz, 1H), 8.35 (d, J = 2.1 Hz, 1H), 8.13 (dd, J = 0, 2.1 Hz, 1H), 7.78 (d, J = 7.5 Hz, 2H), 7.68 (m, 1H), 7.65 (d, J = 8.4 Hz, 1H), 7.53 (t, J = 7.5 Hz, 2H), 7.43–7.35 (m, 2H), 5.61 (s, 2H), 2.21–2.16 (m, 1H), 1.12–1.11 (m, 2H), 0.99–0.94 (m, 2H); ^{13}C NMR (75 MHz, CDCl_3): δ = 162.6, 157.1, 149.0, 148.4, 146.6, 139.6, 139.2, 134.6, 133.3, 132.3, 128.9, 127.7, 127.5, 127.1, 124.8, 123.7, 120.3, 44.3, 14.4, 9.0. HRMS (ESI): m/z calcd for $\text{C}_{23}\text{H}_{20}\text{N}_3\text{O}$ [M + H]⁺ 354.1606; found 354.1599. Melting point: 124–128 °C.

2-Cyclopropyl-6-(2-methoxyphenyl)-3-(pyridin-3-ylmethyl)-quinazolin-4(3H)-one (4b). Chromatography was performed using 70% EtOAc in *n*-hexane to yield a pale yellow solid R_f (70% EtOAc in *n*-hexane) = 0.5; ^1H NMR (300 MHz, DMSO- d_6): δ = 8.60 (s, 1H), 8.50 (s, 1H), 8.20 (d, J = 2.1 Hz, 1H), 7.92 (dd, J = 8.4 Hz, 2.1 Hz, 1H), 7.67 (m, 1H), 7.59 (d, J = 8.4 Hz, 1H), 7.42–7.35 (m, 3H), 7.17 (d, J = 8.4 Hz, 1H), 7.09–7.04 (m, 1H), 5.61 (s, 2H), 3.79 (s, 3H), 2.22–2.14 (m, 1H), 1.12–1.07 (m, 2H), 0.98–0.92 (m, 2H). ^{13}C NMR (75 MHz, CDCl_3): δ = 162.6, 156.9, 156.4, 148.9, 148.3, 146.3, 136.9, 136.1, 134.5, 132.1, 130.8, 129.2, 129.1, 127.3, 126.4, 123.8, 120.9, 119.8, 111.2, 55.5, 44.2, 14.4, 8.9. HRMS (ESI): m/z calcd for $\text{C}_{24}\text{H}_{22}\text{N}_3\text{O}_2$ [M + H]⁺ 384.1712 found 384.1742. Melting point: 85–88 °C.

2-Cyclopropyl-6-(3,4-dimethylphenyl)-3-(pyridin-3-ylmethyl)-quinazolin-4(3H)-one (4c). Chromatography was performed using 70% EtOAc in *n*-hexane to yield a pale yellow solid. R_f (70% EtOAc in *n*-hexane) = 0.55; ^1H NMR (300 MHz, DMSO-

d_6): δ = 8.61 (d, J = 2.1 Hz, 1H), 8.51 (dd, J = 5.1, 1.5 Hz, 1H), 8.32 (d, J = 2.1 Hz, 1H), 8.10 (dd, J = 8.4, 2.1 Hz, 1H), 7.67–7.64 (m, 1H), 7.62 (d, J = 8.4 Hz, 1H), 7.55 (s, 1H), 7.49 (d, J = 8.4 Hz, 1H), 7.39–7.35 (dd, J = 7.5, 4.8 Hz, 1H), 7.27 (d, J = 7.8 Hz, 1H), 5.62 (s, 2H), 2.31 (s, 3H), 2.27 (s, 3H), 2.22–2.14 (m, 1H), 1.11–1.07 (m, 2H), 0.98–0.92 (m, 2H). ^{13}C NMR (75 MHz CDCl_3): δ = 162.6, 156.7, 148.8, 148.2, 146.3, 139.2, 137.1, 137.0, 136.2, 134.7, 133.1, 132.4, 130.1, 128.2, 127.3, 124.3, 123.7, 120.2, 44.2, 19.8, 19.3, 14.3, 8.9. HRMS (ESI): m/z calcd for $\text{C}_{25}\text{H}_{24}\text{N}_3\text{O}$ [M + H]⁺ 382.1919 found 382.1941. Melting point: 176–180 °C.

6-(2-Acetylphenyl)-2-cyclopropyl-3-(pyridin-3-ylmethyl)quinazolin-4(3H)-one (4d). Chromatography was performed using 70% EtOAc in *n*-hexane to yield a pale yellow solid. R_f (70% EtOAc in *n*-hexane) = 0.55; ^1H NMR (400 MHz, CDCl_3): δ = 8.63 (bs, 1H), 8.55 (bs, 1H), 8.28 (bs, 1H), 7.64 (bs, 4H), 7.56 (d, J = 7.4 Hz, 1H), 7.47–7.43 (m, 2H), 7.30–7.26 (m, 1H), 5.62 (s, 2H), 2.16 (s, 3H), 1.91–1.88 (m, 1H), 1.28–1.25 (m, 2H), 1.02–1.01 (m, 2H). ^{13}C NMR (100 MHz, CDCl_3): δ = 203.5, 162.4, 157.6, 149.1, 148.3, 146.9, 140.2, 139.4, 139.1, 135.3, 134.6, 132.2, 131.0, 130.7, 128.2, 127.8, 127.2, 126.4, 123.8, 120.2, 44.3, 30.3, 14.4, 9.2. HRMS (ESI): m/z calcd for $\text{C}_{25}\text{H}_{22}\text{N}_3\text{O}_2$ [M + H]⁺ 396.1712 found 396.1717. Melting point: 130–132 °C.

2-Cyclopropyl-6-(3-fluoro-4-methylphenyl)-3-(pyridin-3-ylmethyl)-quinazolin-4(3H)-one (4e). Chromatography was performed using 70% EtOAc in *n*-hexane to yield a pale yellow solid. R_f (70% EtOAc in *n*-hexane) = 0.55; ^1H NMR (300 MHz, DMSO- d_6): δ = 8.60 (s, 1H), 8.51 (d, J = 3.3 Hz, 1H), 8.35 (d, J = 2.1 Hz, 1H), 8.14 (dd, J = 8.4, 2.1 Hz, 1H), 7.67–7.63 (m, 2H), 7.61 (d, J = 6.3 Hz, 1H), 7.55–7.52 (m, 2H), 7.43–7.35 (m, 2H), 5.62 (s, 2H), 2.28 (s, 3H), 2.20–2.16 (m, 1H), 1.11–1.10 (m, 2H), 0.98–0.95 (m, 2H). ^{13}C NMR (75 MHz, CDCl_3): δ = 163.2, 159.9, 157.2, 149.0, 148.4, 146.7, 139.1, 137.8, 134.6, 134.6, 133.0, 132.2, 131.8, 127.5, 124.5, 123.7, 122.2, 120.2, 113.5, 113.2, 44.3, 14.3, 9.0. HRMS (ESI): m/z calcd for $\text{C}_{24}\text{H}_{21}\text{FN}_3\text{O}$ [M + H]⁺ 386.1669 found 386.1645. Melting point: 120–123 °C.

2-Cyclopropyl-6-(2,6-dichlorophenyl)-3-(pyridin-3-ylmethyl)-quinazolin-4(3H)-one (4f). Chromatography was performed using 70% EtOAc in *n*-hexane to yield a pale yellow solid. R_f (70% EtOAc in *n*-hexane) = 0.55; ^1H NMR (300 MHz, DMSO- d_6): δ = 8.60, (s, 1H), 8.51 (d, J = 3.3 Hz, 1H), 8.39 (d, J = 2.1 Hz, 1H), 8.19 (dd, J = 8.4, 2.1 Hz, 1H), 7.85 (d, J = 1.2 Hz, 2H), 7.68–7.62 (m, 3H), 7.39 (dd, J = 7.8, 5.1 Hz, 1H), 5.62 (s, 2H), 2.23–2.17 (m, 1H), 1.14–1.10 (m, 2H), 0.99–0.95 (m, 2H). ^{13}C NMR (75 MHz, CDCl_3): δ = 162.4, 157.9, 149.1, 148.4, 147.4, 142.5, 136.3, 135.5, 134.7, 132.9, 132.1, 127.9, 127.6, 125.5, 125.2, 123.8, 120.4, 44.4, 14.4, 9.3. HRMS (ESI): m/z calcd for $\text{C}_{23}\text{H}_{18}\text{Cl}_2\text{N}_3\text{O}$ [M + H]⁺ 422.0827; found 422.0847. Melting point: 90–92 °C.

Methyl-4-(2-cyclopropyl-4-oxo-3-(pyridin-3-ylmethyl)-3,4-dihydroquinazolin-6-yl)benzoate (4g). Chromatography was performed using 70% EtOAc in *n*-hexane to yield a pale yellow solid. R_f (70% EtOAc in *n*-hexane) = 0.55; ^1H NMR (300 MHz, DMSO- d_6): δ = 8.61 (s, 1H), 8.51 (d, J = 4.2 Hz, 1H), 8.44 (d, J = 1.8 Hz, 1H), 8.21 (dd, J = 8.4, 2.1 Hz, 1H), 8.09 (d, J = 8.4 Hz, 2H), 7.97 (d, J = 8.4 Hz, 2H), 7.94 (d, J = 8.4 Hz, 1H), 7.68

(m, 1H), 7.66 (d, J = 8.1 Hz, 1H), 7.39 (dd, J = 8.4, 5.2 Hz, 1H), 5.63 (s, 2H), 3.89 (s, 3H), 2.27–2.20 (m, 1H), 1.12 (m, 2H), 0.99 (m, 2H). ^{13}C NMR (75 MHz, CDCl_3): δ = 166.7, 162.5, 157.6, 149.1, 148.4, 147.2, 143.9, 137.7, 134.6, 133.1, 132.1, 130.2, 129.2, 127.7, 126.9, 125.2, 123.7, 120.3, 52.1, 44.3, 14.4, 9.2. HRMS (ESI): m/z calcd for $\text{C}_{25}\text{H}_{22}\text{N}_3\text{O}_3$ [M + H]⁺ 412.1661 found 412.1688. Melting point: 170–174 °C.

4-[2-Cyclopropyl-4-oxo-3-(pyridin-3-ylmethyl)-3,4-dihydroquinazolin-6-yl]benzonitrile (4h). Chromatography was performed using 70% EtOAc in *n*-hexane to yield a pale yellow solid. R_f (70% EtOAc in *n*-hexane) = 0.55; ^1H NMR (300 MHz, DMSO-d₆): δ = 8.61 (s, 1H), 8.51 (d, J = 3.3 Hz, 1H), 8.43 (d, J = 2.1 Hz, 1H), 8.21 (dd, J = 8.4, 2.1 Hz, 1H), 8.02 (d, J = 8.1 Hz, 2H), 7.96 (d, J = 8.1 Hz, 2H), 7.68 (m, 2H), (d, J = 8.1 Hz, 1H), 7.39 (dd, J = 8.4, 5.1 Hz, 1H), 5.62 (s, 2H), 2.22–2.17 (m, 1H), 1.13–1.12 (m, 2H), 0.99–0.95 (m, 2H). ^{13}C NMR (75 MHz, CDCl_3): δ = 162.4, 158.1, 149.2, 148.4, 147.6, 144.0, 136.8, 134.6, 133.0, 132.7, 128.0, 127.6, 125.4, 123.7, 120.5, 118.7, 111.3, 44.4, 14.4, 9.3. HRMS (ESI): m/z calcd for $\text{C}_{24}\text{H}_{19}\text{N}_4\text{O}$ [M + H]⁺ 379.1559 found 379.1561. Melting point: 110–113 °C.

2-Cyclopropyl-6-(3-nitrophenyl)-3-(pyridin-3-ylmethyl)quinazolin-4(3H)-one (4i). Chromatography was performed using 70% EtOAc in *n*-hexane to yield a pale yellow solid. R_f (70% EtOAc in *n*-hexane) = 0.55; ^1H NMR (400 MHz, CDCl_3): δ = 8.64 (s, 1H), 8.54 (s, 3H), 8.24 (d, J = 8.0 Hz, 1H), 8.03 (d, J = 8.0 Hz, 1H), 7.99 (dd, J = 8.4, 2.0 Hz, 1H), 7.71–7.61 (m, 3H), 7.30–7.26 (m, 1H), 5.64 (s, 2H), 1.99–1.90 (m, 1H), 1.31–1.29 (m, 2H), 1.05–1.03 (m, 2H). ^{13}C NMR (100 MHz, CDCl_3): δ = 162.4, 158.0, 149.2, 148.8, 148.4, 147.5, 141.3, 136.4, 134.6, 132.9, 132.0, 129.9, 128.0, 125.3, 123.7, 122.4, 121.8, 120.5, 44.4, 14.4, 9.3. HRMS (ESI): m/z calcd for $\text{C}_{23}\text{H}_{19}\text{N}_4\text{O}_3$ [M + H]⁺ 399.1457 found 399.1460. Melting point: 157–160 °C.

2-Cyclopropyl-6-(4-(dimethylamino)phenyl)-3-(pyridin-3-ylmethyl)quinazolin-4(3H)-one (4j). Chromatography was performed using 70% EtOAc in *n*-hexane to yield a pale yellow solid. R_f (70% EtOAc in *n*-hexane) = 0.55; ^1H NMR (400 MHz, CDCl_3): δ = 8.63 (s, 1H), 8.56 (d, J = 4.0 Hz, 1H), 8.51 (d, J = 1.6 Hz, 1H), 8.0 (dd, J = 8.4, 1.6 Hz, 1H), 7.65 (d, J = 8.4 Hz, 1H), 7.60 (m, 1H), 7.34 (t, J = 8.0 Hz, 1H), 7.29 (dd, J = 8.0, 4.8 Hz, 1H), 7.03 (d, J = 8.0 Hz, 1H), 7.0 (s, 1H), 6.78 (d, J = 8.4 Hz, 1H), 5.63 (s, 2H), 3.02 (s, 6H), 1.91–1.89 (m, 1H), 1.2–1.28 (m, 2H), 1.02–1.0 (m, 2H). ^{13}C NMR (100 MHz, CDCl_3): δ = 162.6, 156.8, 150.9, 148.9, 148.3, 146.5, 141.0, 139.1, 134.6, 133.5, 132.3, 129.5, 127.2, 124.7, 122.9, 120.1, 115.5, 111.9, 111.1, 44.2, 40.6, 14.3, 8.9. HRMS (ESI): m/z calcd for $\text{C}_{25}\text{H}_{25}\text{N}_4\text{O}$ [M + H]⁺ 397.2028 found 397.2011. Melting point: 130–132 °C.

6-(3,5-Bis(trifluoromethyl)phenyl)-2-cyclopropyl-3-(pyridin-3-ylmethyl)quinazolin-4(3H)-one (4k). Chromatography was performed using 70% EtOAc in *n*-hexane to yield a pale yellow solid. R_f (70% EtOAc in *n*-hexane) = 0.55; ^1H NMR (300 MHz, CDCl_3): δ = 8.64 (s, 1H), 8.58 (d, J = 3.3 Hz, 1H), 8.54 (d, J = 2.1 Hz, 1H), 8.11 (s, 2H), 8.0 (dd, J = 8.4, 2.1 Hz, 1H), 7.89 (s, 1H), 7.73 (d, J = 8.4 Hz, 1H), 7.64 (d, J = 7.8 Hz, 1H), 7.31 (dd, J = 7.8, 5.1 Hz, 1H), 5.64 (s, 2H), 1.98–1.90 (m, 1H), 1.33–1.28 (m, 2H), 1.08–1.02 (m, 2H). ^{13}C NMR (75 MHz, CDCl_3): δ = 162.4, 158.3, 149.2, 148.4, 147.7, 141.7, 135.8, 134.6, 132.9,

132.6, 132.1, 128.2, 127.1, 125.5, 123.8, 121.4, 120.6, 44.5, 14.4, 9.4. HRMS (ESI): m/z calcd for $\text{C}_{25}\text{H}_{18}\text{F}_6\text{N}_3\text{O}$ [M + H]⁺ 490.1354 found 490.1349. Melting point: 126–130 °C.

2-Cyclopropyl-6-(4-(methylsulfonyl)phenyl)-3-(pyridin-3-ylmethyl)quinazolin-4(3H)-one (4l). Chromatography was performed using 70% EtOAc in *n*-hexane to yield a pale yellow solid. R_f (70% EtOAc in *n*-hexane) = 0.55; ^1H NMR (400 MHz, CDCl_3): δ = 8.63 (s, 1H), 8.57 (d, J = 4.0 Hz, 1H), 8.54 (d, J = 2.4 Hz, 1H), 8.05 (d, J = 8.4 Hz, 2H), 7.99 (dd, J = 8.4, 2.4 Hz, 1H), 7.89 (d, J = 8.8 Hz, 2H), 7.71 (d, J = 8.8 Hz, 1H), 7.63 (d, J = 8.0 Hz, 1H), 7.31 (dd, J = 7.6, 3.2 Hz, 1H), 5.64 (s, 2H), 3.11 (s, 3H), 1.95–1.91 (m, 1H), 1.31–1.25 (m, 2H), 1.07–1.02 (m, 2H). ^{13}C NMR (100 MHz, CDCl_3): δ = 162.4, 158.1, 149.1, 148.3, 147.5, 145.0, 139.3, 136.7, 134.6, 133.1, 132.0, 128.0, 127.9, 125.5, 123.7, 120.4, 44.5, 29.6, 14.4, 9.3. HRMS (ESI): m/z calcd for $\text{C}_{24}\text{H}_{22}\text{N}_3\text{OS}$ [M + H]⁺ 432.1382 found 432.1385. Melting point: 208–212 °C.

2-Cyclopropyl-6-(2,4-dihydroxyphenyl)-3-(pyridin-3-ylmethyl)quinazolin-4(3H)-one (4m). Chromatography was performed using 70% EtOAc in *n*-hexane to yield a pale yellow solid. R_f (70% EtOAc in *n*-hexane) = 0.55; ^1H NMR (400 MHz, DMSO-d₆): δ = 9.55 (bs, 1H), 9.42 (bs, 1H), 8.58 (bs, 1H), 8.48 (bs, 1H), 8.24 (s, 1H), 7.92 (d, J = 8.0 Hz, 1H), 7.63 (d, J = 7.6 Hz, 1H), 7.51 (d, J = 8.4 Hz, 1H), 7.35 (bs, 1H), 7.15 (d, J = 8.4 Hz, 1H), 6.43 (s, 1H), 6.34 (d, J = 7.6 Hz, 1H), 5.58 (s, 2H), 2.14 (bs, 1H), 1.06 (bs, 2H), 0.92 (d, J = 3.6 Hz, 2H). ^{13}C NMR (100 MHz, DMSO-d₆): δ = 161.7, 158.2, 157.1, 155.3, 148.4, 148.2, 145.0, 136.7, 135.2, 134.3, 132.7, 130.8, 126.1, 125.4, 123.7, 119.3, 117.5, 107.3, 103.0, 43.7, 13.9, 9.0. HRMS (ESI): m/z calcd for $\text{C}_{23}\text{H}_{20}\text{N}_3\text{O}_3$ [M + H]⁺ 386.1505 found 386.1505. Melting point: 258–261 °C.

2-Cyclopropyl-6-(3,4-dihydroxyphenyl)-3-(pyridin-3-ylmethyl)quinazolin-4(3H)-one (4n). Chromatography was performed using 70% EtOAc in *n*-hexane to yield a pale yellow solid. R_f (70% EtOAc in *n*-hexane) = 0.55; ^1H NMR (400 MHz, DMSO-d₆): δ = 8.74 (s, 1H), 8.63 (d, J = 4.8 Hz, 1H), 8.22 (d, J = 2.0 Hz, 1H), 8.03 (dd, J = 8.4, 2.0 Hz, 2H), 7.61–7.53 (m, 2H), 7.14 (d, J = 2.0 Hz, 1H), 7.05 (dd, J = 8.0, 2.0 Hz, 1H), 6.96 (m, 1H), 6.86 (d, J = 8.0 Hz, 1H), 6.64–6.62 (d, J = 7.6 Hz, 1H), 5.66 (s, 2H), 2.18–2.15 (m, 1H), 1.09 (m, 2H), 0.91–0.89 (m, 2H). ^{13}C NMR (100 MHz, DMSO-d₆): δ = 161.7, 156.8, 152.3, 146.7, 145.8, 145.6, 145.2, 139.6, 138.1, 134, 132.3, 129.9, 127.2, 124.8, 122.3, 119.9, 117.7, 116.2, 113.7, 43.7, 13.9, 9.1. HRMS (ESI): m/z calcd for $\text{C}_{23}\text{H}_{20}\text{N}_3\text{O}_3$ [M + H]⁺ 386.1505 found 386.1524. Melting point: 263–266 °C.

2-Cyclopropyl-3-(pyridin-3-ylmethyl)-6-(2,3,4-trihydroxyphenyl)quinazolin-4(3H)-one (4o). Chromatography was performed using 70% EtOAc in *n*-hexane to yield a pale yellow solid. R_f (70% EtOAc in *n*-hexane) = 0.55; ^1H NMR (400 MHz, DMSO-d₆): δ = 9.13 (s, 1H), 8.59 (s, 1H), 8.50 (m, 3H), 8.26 (d, J = 2.0 Hz, 1H), 7.94 (dd, J = 8.4, 2.0 Hz, 1H), 7.64 (d, J = 8.0 Hz, 1H), 7.53 (d, J = 8.4 Hz, 1H), 7.38 (dd, J = 8.0, 4.8 Hz, 1H), 6.69 (d, J = 8.4 Hz, 1H), 6.43 (d, J = 8.8 Hz, 1H), 5.60 (s, 2H), 2.17–2.13 (m, 1H), 1.08–1.06 (m, 2H), 0.95–0.94 (m, 2H). ^{13}C NMR (100 MHz, DMSO-d₆): δ = 161.7, 157.1, 148.4, 148.2, 146.0, 145.1, 144.0, 137.0, 135.3, 134.3, 133.1, 132.7, 126.0, 125.5, 123.7, 119.7, 119.3, 118.6, 107.3, 43.7, 14.0, 9.1. HRMS

(ESI): m/z calcd for $C_{23}H_{20}N_3O_4$ [M + H]⁺ 402.1454 found 402.1459. Melting point: 284–286 °C.

2-Cyclopropyl-6-(naphthalen-1-yl)-3-(pyridin-3-ylmethyl)quinazolin-4(3H)-one (4p). Chromatography was performed using 70% EtOAc in *n*-hexane to yield a pale yellow solid. R_f (70% EtOAc in *n*-hexane) = 0.55; ¹H NMR (400 MHz, CDCl₃): δ = 8.64 (s, 1H), 8.56 (d, J = 4.0 Hz, 1H), 8.42 (d, J = 1.6 Hz, 1H), 7.93–7.90 (m, 2H), 7.88 (dd, J = 8.8, 2.4 Hz, 2H), 7.71 (d, J = 8.4 Hz, 1H), 7.64 (d, J = 7.6 Hz, 1H), 7.57–7.42 (m, 4H), 7.30–7.26 (dd, J = 8.0, 4.8 Hz, 1H), 5.62 (s, 2H), 1.93–1.90 (m, 1H), 1.33–1.28 (m, 2H), 1.06–1.01 (m, 2H). ¹³C NMR (100 MHz, CDCl₃): δ = 162.6, 157.3, 149.1, 148.3, 146.6, 139.0, 138.7, 136.5, 134.6, 133.7, 132.2, 131.3, 128.3, 128.1, 127.9, 127.3, 126.9, 126.3, 125.9, 125.5, 125.3, 123.8, 120.1, 44.3, 14.4, 9.1. HRMS (ESI): m/z calcd for C₂₇H₂₂N₃O [M + H]⁺ 404.1763 found 404.1781. Melting point: 212–215 °C.

2-Cyclopropyl-3-(pyridin-3-ylmethyl)-6-(pyridin-4-yl)quinazolin-4(3H)-one (4q). Chromatography was performed using 70% EtOAc in *n*-hexane to yield a pale yellow solid. R_f (70% EtOAc in *n*-hexane) = 0.55; ¹H NMR (300 MHz, DMSO-d₆): δ = 8.68 (d, J = 6.3 Hz, 2H), 8.61 (d, J = 1.5 Hz, 1H), 8.51 (m, 2H), 8.25 (dd, J = 8.4, 2.1 Hz, 1H), 7.83–7.81 (m, 2H), 7.69 (m, 1H), 7.61 (d, J = 8.4 Hz, 1H), 7.39 (dd, J = 7.8, 4.8 Hz, 1H), 5.63 (s, 2H), 2.27–2.18 (m, 1H), 1.15–1.10 (m, 2H), 1.0–0.96 (m, 2H). ¹³C NMR (75 MHz, CDCl₃): δ = 162.4, 158.2, 150.0, 149.0, 148.2, 147.9, 147.0, 135.7, 134.7, 132.7, 132.1, 128.0, 125.4, 123.8, 121.5, 120.4, 44.4, 14.4, 9.4. HRMS (ESI): m/z calcd for C₂₂H₁₉N₄O [M + H]⁺ 355.1559 found 356.1557. Melting point: 177–180 °C.

2-Cyclopropyl-6-(1*H*-indol-6-yl)-3-(pyridin-3-ylmethyl)quinazolin-4(3H)-one (4r). Chromatography was performed using 70% EtOAc in *n*-hexane to yield a pale yellow solid. R_f (70% EtOAc in *n*-hexane) = 0.55; ¹H NMR (300 MHz, DMSO-d₆): δ = 11.2 (s, 1H), 8.61 (s, 1H), 8.51 (d, J = 4.2 Hz, 1H), 8.35 (d, J = 2.1 Hz, 1H), 8.14 (dd, J = 8.4, 2.1 Hz, 1H), 7.92 (s, 1H), 7.70 (d, J = 7.2 Hz, 1H), 7.63 (d, J = 8.8 Hz, 1H), 7.53–7.46 (m, 2H), 7.41–7.35 (m, 2H), 6.55 (bs, 1H), 5.60 (s, 2H), 2.20–2.16 (m, 1H), 1.14–1.10 (m, 2H), 0.97–0.94 (m, 2H). ¹³C NMR (75 MHz, CDCl₃): δ = 162.8, 156.4, 148.8, 148.2, 145.9, 140.7, 135.5, 134.8, 133.7, 132.5, 132.0, 131.6, 128.4, 127.3, 125.1, 124.5, 123.8, 121.6, 120.2, 119.3, 111.5, 103.0, 44.3, 14.4, 8.8. HRMS (ESI): m/z calcd for C₂₅H₂₁N₄O [M + H]⁺ 393.1715 found 393.1712. Melting point: 205–209 °C.

6-(Benzofuran-2-yl)-2-cyclopropyl-3-(pyridin-3-ylmethyl)quinazolin-4(3H)-one (4s). Chromatography was performed using 70% EtOAc in *n*-hexane to yield a pale yellow solid. R_f (70% EtOAc in *n*-hexane) = 0.55; ¹H NMR (400 MHz, CDCl₃): δ = 8.74 (d, J = 1.6 Hz, 1H), 8.65 (s, 1H), 8.56 (s, 1H), 8.19 (dd, J = 8.4, 1.6 Hz, 1H), 7.64–7.59 (m, 3H), 7.54 (d, J = 8.4 Hz, 1H), 7.30–7.22 (m, 3H), 7.13 (s, 1H), 5.62 (s, 2H), 1.92–1.84 (m, 1H), 1.28–1.22 (m, 2H), 1.04–1.0 (m, 2H). ¹³C NMR (100 MHz, CDCl₃): δ = 162.4, 157.5, 154.9, 154.6, 149.0, 148.3, 147.3, 137.5, 134.7, 130.7, 129.3, 129.0, 128.8, 128.4, 127.6, 124.6, 123.8, 123.0, 122.9, 121.4, 121.0, 120.4, 111.6, 101.2, 44.3, 14.4, 9.2. HRMS (ESI): m/z calcd for C₂₅H₂₀N₃O₂ [M + H]⁺ 394.1556 found 394.1537. Melting point: 175–177 °C.

2-Cyclopropyl-3-(pyridin-3-ylmethyl)-6-(thiophen-3-yl)quinazolin-4(3H)-one (4t). Chromatography was performed using 70% EtOAc in *n*-hexane to yield a pale yellow solid. R_f (70% EtOAc in *n*-hexane) = 0.55; ¹H NMR (300 MHz, DMSO-d₆): δ = 8.61 (d, J = 1.5 Hz, 1H), 8.51 (dd, J = 4.2, 1.5 Hz, 1H), 8.38 (d, J = 2.1 Hz, 1H), 8.18 (dd, J = 8.4, 2.1 Hz, 1H), 8.05 (m, 1H), 7.70 (m, 3H), 7.60 (d, J = 8.4, 1H), 7.40–7.36 (dd, J = 8.4, 5.1 Hz, 1H), 5.61 (s, 2H), 2.22–2.13 (m, 1H), 1.12–1.07 (m, 2H), 0.98–0.92 (m, 2H). ¹³C NMR (75 MHz, CDCl₃): δ = 162.5, 156.8, 148.9, 148.2, 146.3, 140.7, 134.6, 133.8, 132.5, 132.2, 127.4, 126.5, 126.0, 123.7, 120.9, 120.2, 44.2, 14.3, 8.9. HRMS (ESI): m/z calcd for C₂₁H₁₈N₃OS [M + H]⁺ 360.1171 found 360.1159. Melting point: 146–150 °C.

2-Cyclopropyl-6-(3,5-dimethyl-1*H*-pyrazol-4-yl)-3-(pyridin-3-ylmethyl)quinazolin-4(3H)-one (4u). Chromatography was performed using 70% EtOAc in *n*-hexane to yield a pale yellow solid. R_f (70% EtOAc in *n*-hexane) = 0.55; ¹H NMR (300 MHz, DMSO-d₆): δ = 12.39 (s, 1H), 8.60 (d, J = 1.5 Hz, 1H), 8.50 (d, J = 3.6 Hz, 1H), 7.97 (d, J = 2.1 Hz, 1H), 7.74 (dd, J = 8.4, 2.1 Hz, 1H), 7.67 (d, J = 8.4 Hz, 1H), 7.59 (d, J = 8.4 Hz, 1H), 7.39 (dd, J = 8.4, 5.1 Hz, 1H), 5.60 (s, 2H), 2.23 (s, 6H), 2.19–2.12 (m, 1H), 1.09–1.09 (m, 2H), 0.96–0.92 (m, 2H). ¹³C NMR (75 MHz, CDCl₃): δ = 162.5, 156.8, 149.0, 148.3, 145.8, 142.1, 135.6, 134.6, 132.3, 132.2, 127.1, 126.7, 123.7, 120.2, 117.4, 44.3, 14.4, 11.6, 9.0. HRMS (ESI): m/z calcd for C₂₂H₂₂N₅O [M + H]⁺ 372.1824 found 372.1837. Melting point: 138–141 °C.

2-Cyclopropyl-6-(3,5-dimethylisoxazol-4-yl)-3-(pyridin-3-ylmethyl)quinazolin-4(3H)-one (4v). Chromatography was performed using 70% EtOAc in *n*-hexane to yield a pale yellow solid. R_f (70% EtOAc in *n*-hexane) = 0.55; ¹H NMR (400 MHz, CDCl₃): δ = 8.64 (bs, 1H), 8.57 (bs, 1H), 8.16 (d, J = 2.0 Hz, 1H), 7.67 (d, J = 8.4 Hz, 1H), 7.64–7.62 (m, 1H), 7.62 (dd, J = 8.8, 2.0 Hz, 1H), 7.31 (bs, 1H), 5.62 (s, 2H), 2.44 (s, 3H), 2.30 (s, 3H), 1.96–1.90 (m, 1H), 1.30–1.25 (m, 2H), 1.07–1.04 (m, 2H). ¹³C NMR (100 MHz, CDCl₃): δ = 165.6, 162.2, 158.4, 157.6, 149.0, 148.2, 146.6, 134.9, 134.6, 132.1, 128.5, 127.6, 126.9, 123.7, 120.3, 115.6, 44.3, 14.3, 11.5, 10.7, 9.2. HRMS (ESI): m/z calcd for C₂₂H₂₁N₄O₂ [M + H]⁺ 373.1665 found 373.1685. Melting point: 151–155 °C.

2,6-Dicyclopropyl-3-(pyridin-3-ylmethyl)quinazolin-4(3H)-one (4w). Chromatography was performed using 70% EtOAc in *n*-hexane to yield a pale yellow solid. R_f (70% EtOAc in *n*-hexane) = 0.5; ¹H NMR (400 MHz, CDCl₃): δ = 8.62 (s, 1H), 8.55 (d, J = 3.2 Hz, 1H), 7.93 (d, J = 2.0 Hz, 1H), 7.60 (d, J = 8.0 Hz, 1H), 7.50 (d, J = 8.4 Hz, 1H), 7.46 (dd, J = 8.4, 2.0 Hz, 1H), 7.28–7.25 (m, 1H), 5.60 (s, 2H), 2.05–1.98 (m, 1H), 1.89–1.83 (m, 1H), 1.25–1.19 (m, 2H), 1.06–0.98 (m, 2H), 0.97–0.95 (m, 2H), 0.81–0.77 (m, 2H); ¹³C NMR (100 MHz, CDCl₃): δ = 162.6, 155.9, 148.8, 148.2, 145.4, 142.8, 134.8, 132.5, 126.9, 123.8, 122.5, 119.3, 118.3, 44.2, 15.3, 14.4, 9.7, 8.7; HRMS (ESI): m/z calcd for C₂₀H₂₀N₃O [M + H]⁺ 318.1606; found 318.1614. Melting point: 77–79 °C.

2-Cyclopropyl-6-isobutyl-3-(pyridin-3-ylmethyl)quinazolin-4(3H)-one (4x). Chromatography was performed using 70% EtOAc in *n*-hexane to yield a pale yellow solid. R_f (70% EtOAc in *n*-hexane) = 0.55; ¹H NMR (400 MHz, CDCl₃): δ = 8.62

(bs, 1H), 8.55 (bs, 1H), 8.04 (s, 1H), 7.60 (d, $J = 8.4$ Hz, 1H), 7.53–7.49 (m, 2H), 7.28 (m, 1H), 5.60 (s, 2H), 2.61 (d, $J = 7.2$ Hz, 2H), 1.97–1.90 (m, 1H), 1.89–1.84 (m, 1H), 1.23–1.20 (m, 2H), 1.0–0.95 (m, 2H), 0.92 (d, $J = 6.0$ Hz, 6H). ^{13}C NMR (100 MHz, CDCl_3): $\delta = 162.7, 156.2, 149.0, 148.4, 145.7, 140.3, 135.8, 134.6, 132.5, 126.7, 126.4, 123.7, 119.7, 45.0, 44.2, 30.2, 22.2, 14.3, 8.7$. HRMS (ESI): m/z calcd for $\text{C}_{21}\text{H}_{24}\text{N}_3\text{O} [\text{M} + \text{H}]^+$ 334.1919 found 334.2566. Melting point: 110–113 °C.

2-Cyclopropyl-6-methyl-3-(pyridin-3-ylmethyl)quinazolin-4-(3H)-one (4y). Chromatography was performed using 70% EtOAc in *n*-hexane to yield a pale yellow solid. R_f (70% EtOAc in *n*-hexane) = 0.55; ^1H NMR (400 MHz, CDCl_3): $\delta = 8.61$ (s, 1H), 8.54 (d, $J = 4.4$ Hz, 1H), 8.07 (s, 1H), 7.59 (d, $J = 8.0$ Hz, 1H), 7.55 (dd, $J = 8.0, 2.0$ Hz, 1H), 7.49 (d, $J = 8.0$ Hz, 1H), 7.27 (dd, $J = 8.0, 4.4$ Hz, 1H), 5.60 (s, 2H), 2.47 (s, 3H), 1.90–1.83 (m, 1H), 1.25–1.20 (m, 2H), 1.0–0.95 (m, 2H). ^{13}C NMR (100 MHz, CDCl_3): $\delta = 162.6, 156.2, 149.0, 148.3, 145.4, 136.5, 135.9, 134.6, 132.4, 126.8, 126.3, 123.7, 119.8, 44.2, 21.2, 14.4, 8.7$. HRMS (ESI): m/z calcd for $\text{C}_{18}\text{H}_{18}\text{N}_3\text{O} [\text{M} + \text{H}]^+$ 292.1450 found 292.1440. Melting point: 98–100 °C.

Assay of α -glucosidase inhibitory activity

The inhibitory effect of the synthesized compounds on α -glucosidase was evaluated in 96-well plates employing the substrate PNPG and 4-nitrophenyl α -D-glucopyranoside according to the procedure previously reported.²¹ Prior to use, all test compounds were solubilized in solvent, dimethylsulfoxide (DMSO), and then further diluted in DMSO to acquire the desired final maximum test concentration. In brief, each well comprised substrate 4-nitrophenyl α -D-glucopyranoside in 2 mM phosphate buffer (pH 7.2) and different test concentrations (10–100 $\mu\text{g mL}^{-1}$). The reaction was commenced by the addition of enzyme (0.1 IU per well), α -glucosidase (obtained from Sigma Aldrich, Bengaluru) and the plates were incubated at 37 °C for 10 min. The absorbance was measured spectrophotometrically at 410 nm (Spectra MAX Plus; Molecular Devices; supported by SOFTmax PRO-3.0). The increase in absorbance (ΔA) was compared with that of control (buffer instead of test compound) to compute the inhibitory activity of enzyme. The half maximal inhibitory concentrations (IC_{50}) were determined from two independent assays, performed in duplicate. Acarbose, an illustrious inhibitor of α -glucosidase was employed as positive control.

$$\text{Inhibition (\%)} = (\Delta A_{\text{control}} - \Delta A_{\text{sample}})/\Delta A_{\text{control}} \times 100\%$$

The concentration of inhibition required for 50% of α -glucosidase activity under the assay conditions was defined as the IC_{50} value.

Inhibitions kinetics

There are a variety of methods available to compute the inhibition constant (K_i) that characterizes substrate inhibition by a competitive inhibitor. Among them, the Dixon plot is frequently employed to investigate the mechanism of inhibition

and estimate the K_i of the reaction. The plots were prepared of the reciprocal of rate of product formation ($1/v$) versus the inhibitor concentration at different substrate concentrations.²² The relationship is follows as,

$$1/v = (K_m [I]/V_{\text{max}} [S]K_i) + 1/V_{\text{max}} (1 + K_m/[S])$$

The subsequent straight lines were analyzed by linear regression using the ORIGIN (version 8) software. The K_i values were obtained by simultaneously interpreting two sets of equations successively; one equation for each of the straight lines equated with the line that represented the highest substrate concentration (this line has the smallest slope). The point of intersection of these pairs of lines signifies the value of K_i . The latter values are reported as means or as a range of values.

Acknowledgements

Authors are grateful to GVK Biosciences Pvt Ltd, for the financial support and encouragement. We thank Prof. Mahesh K. Lakshman, Department of Chemistry, The City College and The City University of New York, New York, USA for his invaluable support and motivation.

References

- Y. Yoshikawa, R. Hirata, H. Yasui and H. Sakurai, *Biochimie*, 2009, **91**, 1339.
- (a) L. M. Tierney, S. J. McPhee and M. A. Papadakis, *Current Medical Diagnosis and Treatment, International Edition*, Lange Medical Books McGraw-Hill, New York, 2002, p. 1203; (b) K. I. Rother, *N. Engl. J. Med.*, 2007, **356**, 1499.
- D.-Q. Li, Z.-M. Qian and S.-P. Li, *J. Agric. Food Chem.*, 2010, **58**, 6608.
- (a) S. Onal, S. Timur, B. Okutucu and F. Zihnioglu, *Prep. Biochem. Biotechnol.*, 2005, **35**, 29; (b) D. M. Casirola and R. P. Ferraris, *Metabolism*, 2006, **55**, 832.
- (a) A. Trapero and A. Llebaria, *J. Med. Chem.*, 2012, **55**, 10345; (b) S. B. Ferreira, A. C. R. Sodero, M. F. C. Cardoso, E. S. Lima, C. R. Kaiser, F. P. Silva and V. F. Ferreira, *J. Med. Chem.*, 2010, **53**, 2364; (c) J. Xiao, W. Westbroek, O. Motabar, W. A. Lea, X. Hu, A. Velayati, W. Zheng, N. Southall, A. M. Gustafson, E. Goldin, E. Sidransky, K. Liu, A. Simeonov, R. J. Tamargo, A. Ribes, L. Matalonga, M. Ferrer and J. J. Marugan, *J. Med. Chem.*, 2012, **55**, 7546; (d) A. Kato, E. Hayashi, S. Miyauchi, I. Adachi, T. Imahori, Y. Natori, Y. Yoshimura, R. J. Nash, H. Shimaoka, I. Nakagome, J. Koseki, S. Hirono and H. Takahata, *J. Med. Chem.*, 2012, **55**, 10347.
- (a) A. Mehta, N. Zitzmann, P. M. Rudd, T. M. Block and R. A. Dwek, *FEBS Lett.*, 1998, **430**, 17–22; (b) E. Simsek, X. Lu, S. Ouzounov, T. M. Block and A. S. Mehta, *Antiviral Chem. Chemother.*, 2006, **17**, 259–267; (c) A. Mehta,

- P. M. Rudd, T. M. Block and R. A. Dwek, *Biochem. Soc. Trans.*, 1997, **25**, 188–193; (d) S. B. Oppenheimer, M. Alvarez and J. Nnoli, *Acta Histochem.*, 2008, **110**, 6–13.
- 7 Z.-K. Wan, S. Wacharasindhu, C. G. Levins, M. Lin, K. Tabei and T. S. Mansour, *J. Org. Chem.*, 2007, **72**, 10194.
- 8 (a) S. Patterson, M. S. Alphéy, D. C. Jones, E. J. Shanks, I. P. Street, J. A. Frearson, P. G. Wyatt, I. H. Gilbert and A. H. Fairlamb, *J. Med. Chem.*, 2011, **54**, 6514; (b) A. M. Al-Obaid, S. G. Abdel-Hamid, H. A. El-Kashef, A. A.-M. Abdel-Aziz, A. S. El-Azab, H. A. Al-Khamees and H. I. El-Subbagh, *Eur. J. Med. Chem.*, 2009, **44**, 2379.
- 9 T. P. Selvam and P. V. Kumar, *Res. Pharm.*, 2011, **1**, 1.
- 10 (a) J.-F. Liu, J. Lee, A. D. Dalton, G. Bi, L. Yu, C. M. Baldino, E. McElroy and M. Brown, *Tetrahedron Lett.*, 2005, **46**, 1241; (b) P. M. Chandrika, T. Yakaiah, A. R. R. Rao, B. Narsaiah, N. C. Reddy, V. Sridhar and J. V. Rao, *Eur. J. Med. Chem.*, 2008, **43**, 846; (c) F. Rorsch, E. L. Buscato, K. Deckmann, G. Schneider, M. Schubert-Zsilavecz, G. Geisslinger, E. Proschak and S. Grosch, *J. Med. Chem.*, 2012, **55**, 3792; (d) H. Hikawa, Y. Ino, H. Suzuki and Y. Yokoyama, *J. Org. Chem.*, 2012, **77**, 7046.
- 11 R. Garlapati, N. Pottabathini, V. Gurram, A. B. Chaudhary, V. R. Chunduri and B. Patro, *Tetrahedron Lett.*, 2012, **53**, 5162.
- 12 (a) J. Rudolph, W. P. Esler, S. O. Connor, P. D. G. Coish, P. L. Wickens, M. Brands, D. E. Bierer, B. T. Bloomquist, G. Bondar, L. Chen, C.-Y. Chuang, T. H. Claus, Z. Fathi, W. Fu, U. R. Khire, J. A. Kristie, X.-G. Liu, D. B. Lowe, A. C. McClure, M. Michels, A. A. Ortiz, P. D. Ramsden, R. W. Schoenleber, T. E. Shelekhin, A. Vakalopoulos, W. Tang, L. Wang, L. Yi, S. J. Gardell, J. N. Livingston, L. J. Sweet and W. H. Bullock, *J. Med. Chem.*, 2007, **50**, 5202; (b) C. A. Mosley, T. M. Acker, K. B. Hansen, P. Mullaseril, K. T. Andersen, P. Le, K. M. Vellano, H. Brauner-Osborne, D. C. Liotta and S. F. Traynelis, *J. Med. Chem.*, 2010, **53**, 5476.
- 13 (a) B. W. Surber, J. L. Cross and S. M. Hannick, *J. Labelled Compd. Radiopharm.*, 2010, **53**, 468; (b) M. Zhang, X. Cui, X. Chen, L. Wang, J. Li, Y. Wu, L. Hou and Y. Wu, *Tetrahedron*, 2012, **68**, 900.
- 14 (a) C. C. Johansson Seechurn, M. O. Kitching, T. J. Colacot and V. Snieckus, *Angew. Chem., Int. Ed.*, 2012, **51**, 5062; (b) H. Li, C. C. Johansson Seechurn and T. J. Colacot, *ACS Catal.*, 2012, **2**, 1147; (c) J. W. Grate and G. C. Frye, in *Sensors Update*, ed. H. Baltes, W. Göpel and J. Hesse, Wiley-VCH, Weinheim, 1996, vol. 2, p. 10; (d) A. Suzuki, in *Metal-Catalyzed Cross-Coupling Reactions*, ed. F. Diederich and P. J. Stang, Wiley-VCH, New York, 1998, p. 49; (e) N. Miyaura, *Top. Curr. Chem.*, 2002, **219**, 11; (f) J. Tsuji, *Palladium Reagents and Catalysts: New Perspectives for the 21st Century*, John Wiley and Sons, 2004, p. 288; (g) A. Suzuki, in *Boronic Acids: Preparation and Applications in Organic Synthesis and Medicine*, ed. D. G. Hall, Wiley-VCH, Weinheim, 2005, p. 123; (h) For a review of the Suzuki–Miyaura reactions of heteroaryl boronic acids, see: E. Tyrrell and P. Brookes, *Synthesis*, 2004, 469.
- 15 (a) V. Gurram, N. Pottabathini, R. Garlapati, A. B. Chaudhary, B. Patro and M. K. Lakshman, *Chem.–Asian J.*, 2012, **7**, 1853; (b) R. Pratap, D. Parrish, P. Gunda, D. Venkatramana and M. K. Lakshman, *J. Am. Chem. Soc.*, 2009, **131**, 12240.
- 16 (a) M. K. Lakshman, P. Gunda and P. Pradhan, *J. Org. Chem.*, 2005, **70**, 10329; (b) C. Liu, Q. Ni, F. Bao and J. Qiu, *Green Chem.*, 2011, **13**, 1260.
- 17 (a) V. H. Lillelund, H. H. Jensen, X. Liang and M. Bols, *Chem. Rev.*, 2002, **102**, 515; (b) S. Park, S. Hyun and J. Yu, *Bioorg. Med. Chem. Lett.*, 2011, **21**, 2441; (c) W. Worawalai, S. Wacharasindhu and P. Phuwaprasisirisan, *Med. Chem. Commun.*, 2012, **3**, 1466; (d) Z.-Y. Du, R.-R. Liu, W.-Y. Shao, X.-P. Mao, L. Ma, L.-Q. Gu, Z.-S. Hunng and A. S. C. Chan, *Eur. J. Med. Chem.*, 2006, **41**, 213; (e) H. Wataru, K. Masaaki, O. Haruhiro, N. Toshiyuki and O. Tadatake, *Curr. Top. Med. Chem.*, 2009, **9**, 3.
- 18 (a) A. Sali and T. L. Blundell, *J. Mol. Biol.*, 1993, **234**, 779; (b) A. Fiser, R. K. G. Do and A. Sali, *Protein Sci.*, 2000, **9**, 1753.
- 19 (a) U. Saqib and M. I. Siddiqui, *Int. J. Integr. Biol.*, 2008, **2**, 116; (b) S. Nakamura, K. Takahira, G. Tanabe, O. Muraoka and I. Nakanishi, *Open J. Med. Chem.*, 2012, **2**, 50.
- 20 F. Brindis, R. Rorriguez, R. Bye, M. G. Andrade and R. Mata, *J. Nat. Prod.*, 2011, **74**, 314.
- 21 F. Ferreres, A. Gil-Izquierdo, J. Vinholes, S. T. Silva, P. Valentao and P. B. Andrade, *Food Chem.*, 2012, **134**, 894.
- 22 T. Kakkar, H. Boxenbaum and M. Mayersohn, *Drug Metab. Dispos.*, 1999, **27**, 756.